THREE-DIMENSIONAL RECONSTRUCTION OF SERIAL HISTOLOGICAL MOUSE BRAIN SECTIONS

M. Mallar Chakravarty [1] *, Barry J. Bedell* [1,2] *, Simone P. Zehntner* [1] *Alan C. Evans* [1,2]*, and D. Louis Collins* [1]

[1] McConnell Brain Imaging Centre
Montreal Neurological Institute
3801 University Street, Montreal, Quebec
Canada, H3A 2B4

[2] Neuralyse Inc.
6100 avenue Royalmount
Montreal, Quebec
Canada H4P 2R2

ABSTRACT

Animal models are widely used to improve our understanding of the complex pathophysiological processes underlying diseases of the central nervous system (CNS), as well as a providing a means of evaluating the efficacy of new therapeutic agents. The advent of high-resolution, dedicated small animal magnetic resonance imaging and positron emission tomography scanners has greatly improved the value of animal imaging for such studies. However, the use of *in vivo* imaging markers requires extensive validation against gold standard, *ex vivo* tissue studies. In this paper, we describe methods for three-dimensional reconstruction of two-dimensional serial histological sections to create volumetric data, a major step in the use of *ex vivo* data for validating *in vivo* imaging techniques.

Index Terms— Magnetic Resonance Imaging, Microscopy, Microscopy, Confocal

1. INTRODUCTION

Animal models are often used in the study of disease. Dissection and histological studies help to understand the often complex pathophysiological processes underlying disease. Such studies are also used to evaluate the efficacy of new therapeutic agents and are generally considered the gold standard for the analyses of the natural evolution of pathology or response to therapeutic intervention. However the high morbidity and large number of animals required for each survival study warrants the use of alternative strategies. High-resolution, dedicated small animal magnetic resonance imaging (MRI) and positron emission tomography (PET) scanners have greatly increased the use of animal imaging for studies of disease and therapeutic efficacy since non-invasive *in vivo* imaging offers a powerful means to visualize pathology in living animals and enables longitudinal studies of the same animal [5, 10–12].

However, novel image acquisition and image processing techniques require extensive validation against gold-standard *ex vivo* specimens. To this end we have developed fully-automated techniques for the three-dimensional (3D) reconstruction of two-dimensional (2D) serial histological sections from the mouse brain. The reconstructed volume is directly mapped onto *in vivo* anatomical MRI volumes. This mapping enables rigorous validation of new imaging techniques, as well as the seamless integration of *ex vivo* molecular and histopathalogical data with *in vivo* structural and functional imaging data [1–3, 8, 9, 13, 16].

The reconstruction techniques described were extended from those developed in Chakravarty *et al.* [3] for the reconstruction of the human basal ganglia and thalamus. In the original work, histological sections were manually aligned and colour balanced, prior to further refinement using non-linear correction techniques. In addition, no blockface or volumetric imaging reference was used in the reconstruction process. In the following sections the reconstruction techniques are extended to ensure that all image processing steps are fully automated.

2. MATERIALS AND METHODS

When histological data is simply stacked, the resultant volume is inhomogeneous with respect to morphology and intensity. The reconstruction of 2D serial histological sections to develop a 3D histological volume is non-trivial and requires

the rigorous acquisition of serial histological data, as well as robust automated processing techniques of the digitized tissue sections. Typically, histological reconstruction requires the use of two, if not all of, the following steps:

1. Slice-to-blockface registration to further minimize the structural inhomogeneities of a single slice. We define the blockface to be the photograph of the volume prior to the acquisition of a single slice of histological data. The blockface serves as a local reference for the single slice.
2. Slice-to-slice registration techniques to minimize structural inhomogeneities between slices.
3. Reconstructed volume to global reference warping to correct global structural inhomogeneities. Global references may include MRI, Computed Tomography or PET data.

In this section, the steps for data acquisition and reconstruction of serial histological sections (using the above steps) are described.

2.1. Data Acquisition

Proper data acquisition is a crucial component of this work. Mouse brains were fixed in neutral-buffered formalin and embedded in blue dyed paraffin to create background-to-foreground contrast. 5 μm sections were cut on a rotary microtome with a gap of 100 μm between each section. A digital blockface image was acquired for each section with a Canon 20D camera equipped with a 100mm macro lens and a 35mm extension tube (yielding images of 3504 x 2336 pixels with field of view which is relatively large with respect to the blockface). The camera was permanently mounted throughout the data acquisition process to limit translation and rotational slice-to-slice differences in the digital blockface. Tissue sections were stained with Luxol fast blue/Hematoxylin & Eosin (H&E) on an automated tissue stainer (Shandon Varistain XY) to achieve high-contrast between anatomical structures. The sections were digitized using Nikon 55i microscope equipped with a 1x objective lens and a QICAM Fast 1394 camera (yielding images of 1392 x 1040 pixels). A total of 120 slices of serial histological data were acquired from a single mouse. An example of the digital blockface and corresponding histological image is shown in Fig. 1.

A three-dimensional anatomical reference volume derived from the average of 10 T2-weighted MRI volumes of mice was used as the volumetric reference for this study [11]. The use of standardized anatomical MRI template has been successfully utilized in histological reconstructions of the human brain [3, 4].

2.2. Linear Histology-to-Blockface alignment

Proper alignment of histological sections to the corresponding blockface image was a two-step process. In the first step, a slice-to-slice alignment of the blockface data was performed. The red channel of the colour blockface image was extracted from the blockface image to enhance foreground-to-background contrast. For the n slices in the volume, $n-1$ transformations (two translations per transformation) were estimated. The center slice ($m = ceil((n-1)/2)$) was chosen as the reference. For all slices $i > m$, a transformation mapping slice i to slice $i-1$ was estimated. Similarly, when $i < m$ a transformation mapping slice i to slice $i+1$ was estimated. For all n slices of the histological data set, a linear transformation (two translations and one rotation per transformation) mapping the slice of histological data to the corresponding slice in the reconstructed blockface volume was estimated and applied. All two-dimensional transformations were estimated using an adapted version of the linear registration technique described by Collins *et al.* [7].

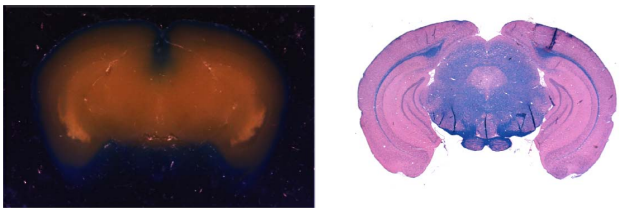

Fig. 1. **Examples of blockface and histological data used for volumetric reconstruction. Left:** Block embedded in black dark blue paraffin block to enhance foreground and background contrast. **Right:** Histological section stained with Luxol fast blue/H&E to create white and grey matter contrast.

2.3. Nonlinear Morphological Correction

Slice-to-slice warping was used to correct for morphological inconsistencies between slices by furthering the techniques previously developed in [3]. In the original work, two nonlinear transformations were estimated at every slice, mapping each slice to the slices occurring immediately before and after it in the series. These transformations were averaged and then applied.

The ANIMAL algorithm was used to for the estimation of nonlinear transformations [6]. ANIMAL is an iterative algorithm which estimates a 3D deformation field on a lattice of nodes which matches a source volume to a target volume. The transformation estimation consists of two steps: the first is the estimation of a translation at each node which maximizes the local similarity measure; the second is a smoothing step to ensure that a continuous deformation field has been estimated. For further details on ANIMAL's parameters, the reader is referred to [3, 6].

Global volumetric morphological consistency was achieved by enforcing local slice-to-slice morphological consistency. Here ANIMAL was modified to estimate eight 2D nonlinear transformations at each slice: the first four transformations

matching slice i to the four slices which came before it in the series (slices $i-1$, $i-2$, $i-3$, and $i-4$) and the second four transformations estimated match slice i to the 4 slices that came after it in the series (slices $i+1$, $i+2$, $i+3$, and $i+4$). These transformations were averaged and then applied to slice i, thus regularizing the slice-to-slice nonlinear warp throughout the volume.

For each slice-to-slice transformation, a hierarchical strategy was used, where images were convolved with a Gaussian kernel of large full-width at half-maximum (FWHM) in order to recover large deformations. These deformations were then used as the input transformation to the next transformation step, where images were blurred with a Gaussian kernel of smaller FWHM in order to recover smaller deformations. Stiffness, weight, and similarity parameters used were the same as those optimized in [3]. Other parameters, such as the FWHM, step, and sub-lattice diameter, were scaled from the original parameters presented in [3] The slice-to-slice nonlinear registration parameters used for transformation estimation are given in Table 2. Each slice-to-slice nonlinear transformation was stored and utilized in the intensity correction scheme presented in the next section.

Table 1. ANIMAL parameters used for slice-to-slice nonlinear transformation estimation.

FWHM (mm)	Step Size (mm)	Sub Lattice Diameter (mm)	Sub Lattice	Iterations
0.5	0.5	1.5	25	50
0.25	0.25	1	15	50
0.1	0.1	0.5	15	50
0.05	0.05	0.1	12	50

2.4. Nonlinear Intensity Correction

Slice-to-slice intensity inhomogeneities can occur due to varying staining density and local differences in slice thickness. These differences will result in a histological volume which is inhomogeneous in slice-to-slice intensities, making the visualization of anatomical structures difficult.

The intensity correction procedure initially uses the nonlinear transformations estimated in the previous section. The inverse of the transformations estimated matching slice i to the four slices before it and the four slices after it in the series were applied so that all slices were morphologically consistent. Each slice was then partitioned into a series of square neighborhoods of equal size. The assumption utilized was that if each neighborhood was small enough, then a first-order polynomial scaling factor can be estimated to match the joint histograms of the neighborhoods by using a least-trimmed squares polynomial estimation [14]. Thus, for each neighborhood, eight different scaling factors were estimated, then averaged and stored in a grid. Each scaling factor matched the neighborhood of slice i to the analogous neighborhoods in slices $i-1$ to $i-4$, and slices $i+1$ to $i+4$ (after spatial transformation). Square neighborhoods of 0.3mm were used for the mouse data presented here. Once this was done for each neighborhood, the resultant grid was interpolated using a bicubic kernel to match the resolution of the histological image. Slice i was then multiplied by the interpolated field to improve slice-to-slice grey-level consistency.

2.5. Warping Histological Volume to an MRI Template

The MRI-template used is a nonlinear average of twelve T2-weighted mouse MRI volumes developed by Lau *et al*. [11] with 0.156 mm isotropic voxels. The T2 volume contains similar contrast to the histology (high intensity grey matter, low intensity white matter, and extremely high intensity cerebrospinal fluid). Thus,the reconstructed histological volume can be warped to the volume directly. The histological volume was masked using a simple threshold and morphological operators (keeping largest connected component, and erosion and dilation). Linear alignment was first achieved using a modified version of [7]. A hierarchical 3D nonlinear transformation estimation strategy was used using the optimized values for stiffness, weight, and similarity estimated in [15]. The multi-resolution registration parameters are given in Table 2.

Table 2. ANIMAL parameters used for histological volume to MRI template nonlinear transformation estimation.

FWHM (mm)	Step Size (mm)	Sub Lattice Diameter (mm)	Sub Lattice	Iterations
0.5	0.5	0.75	8	20
0.3	0.3	0.5	8	20
0.2	0.2	0.4	8	20

3. RESULTS

Results of the blockface reconstruction, histological alignment to the blockface, nonlinear morphological correction, and nonlinear intensity correction are presented in Fig. 2. Results from the warping of the reconstructed mouse volume to the MRI template is presented in Fig. 3. Results demonstrate proper alignment of the histological volume with the MRI template, however some problems can be observed in the cerebellum, likely due to the relatively low sampling in the slice direction (and the anisotropic dimensions of the volume (1392 x 1040 x 120). This problem could be resolved by

acquiring more histological sections, at the expense of sectioning and computational time.

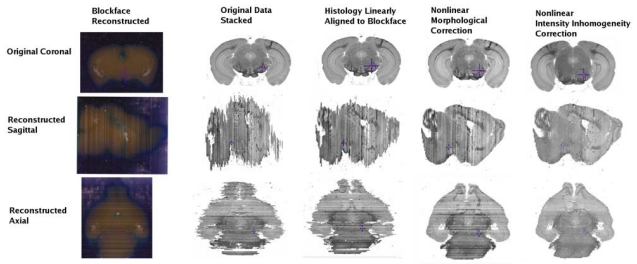

Fig. 2. **Reconstruction of Serial Histological Data. From Left to Right:** Blockface data reconstructed, original histological data stacked without any intensity or morphological correction, reconstruction after slice-to-blockface linear alignment, reconstruction after nonlinear morphological correction, and reconstructions after nonlinear intensity correction.

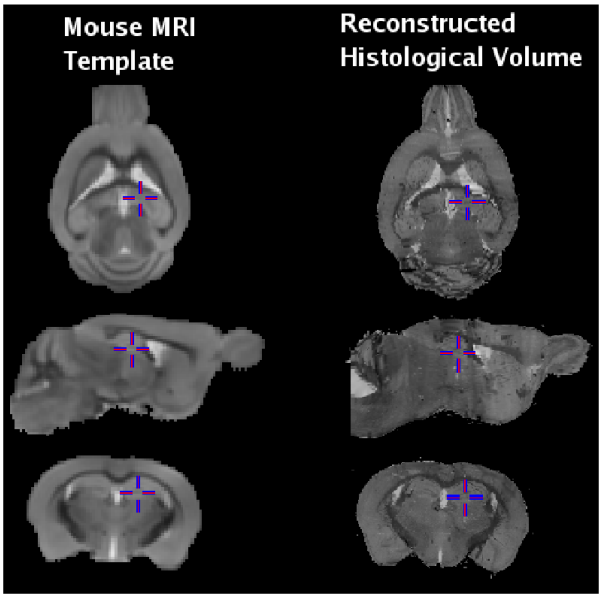

Fig. 3. **Histological Volume Warped to Match MRI-Template.** Original MRI template (left), histological volume warped to match the template (right).

4. CONCLUSIONS

The work presented here discusses the extension of techniques presented in [3, 4] for the reconstruction of serial histological sections from mouse brains. Results demonstrate contiguous anatomical histological volumes, which have been intensity corrected and warped to an MRI-template to account for global morphological differences. We have, demonstrated the use of a fully-automated algorithm for the reconstruction of serial, thin (5 μm) paraffin-embedded brain tissue sections and accurate mapping onto a standardized MRI atlas. The seamless combination of rigorous, high-throughput tissue preparation techniques and automated image processing will allow for a comprehensive, multi-modal, multi-scale evaluation of the natural evolution of pathology or response to therapeutic intervention in rodent models of CNS disease. Future work will involve validating these techniques on more datasets to demonstrate the repeatability of these techniques, as well as application to immunohistochemistry and in-situ hybridization data..

5. REFERENCES

[1] J. Annese *et al. NeuroImage*, 30:61–89, 2006.

[2] U. Burgel *et al. NeuroImage*, 29:1092–1105, 2006.

[3] M.M. Chakravarty *et al. NeuroImage*, 30(2):359–376, 2006.

[4] M.M. Chakravarty *et al.* In *MICCAI 2005*, volume 2 of *LNCS*: 394–401, Palm Springs, USA, October 2005. Springer.

[5] X.J. Chen *et al. NeuroImage*, 29:99–105, 2005.

[6] D.L. Collins and A.C. Evans. *International Journal of Pattern Recognition and Artificial Intelligence*, pages 1271–1294, December 1997.

[7] D.L. Collins *et al. J. of Computer Assisted Tomography*, 18(2):192–205, March 1994.

[8] S. Geyer *et al.* Journal of Anatomy and Embryology 204(4):351–366, 2001.

[9] C. Grefkes *et al. NeuroImage*, 14:617–631, 2001.

[10] N. Kovacevic *et al. Cerebral Cortex*, 15:639–645, 2005.

[11] J.C. Lau *et al.* In *10th International Conference on Alzheimer's Disease and Related Disorders*, Madrid, Spain, 2006.

[12] A. MacKenzie-Graham *et al. Journal of Anatomy*, pages 93–102, 2004.

[13] G. Malandain *et al. Neuroimage*, 23(1).

[14] S. Prima *et al.* In MICCAI'2001, volume 2208 of *LNCS*, pages 811–819, Utrecht, Netherlands, October 2001. Springer.

[15] S. Robbins *et al. Medical Image Analysis*, 8:311–323, 2004.

[16] J. Yelnik *et al. NeuroImage*, 34:618–638, 2007.